

Contents

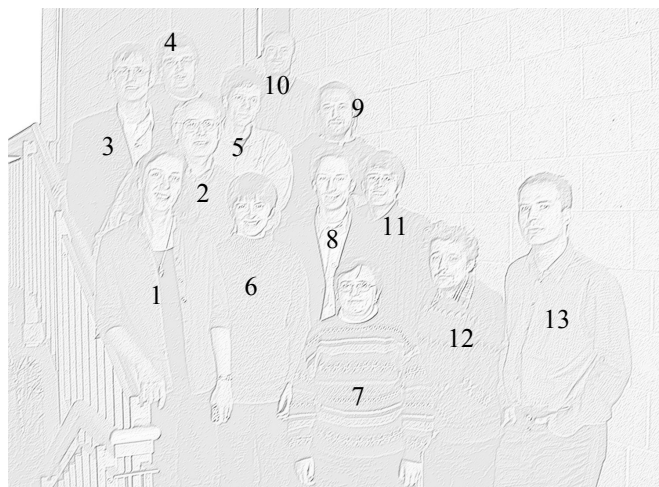
A. Foreword	2
B. Members of the chair of Optoelectronics	3
C. Reports	
1. Characterization of SU-8 photoresist for alignment applications	4
2. Micro-integration of optical modules for angle division multiplexing	5
3. Integrated guiding structures for automatic alignment with μm-accuracy	6
4. Purely optical sensor for absolute measurement of translation and rotation	7
5. Investigation of collimation properties of microlenses	8
6. Parallel method for testing an array of micro lenses	9
7. Alignment through a thick substrate	10
8. Phase screens for astronomical applications	11
9. Improvement of power efficiency by two-dimensional beam shaping	12
10. Calculation of surfaces from ray directions	13
11. Polarisation analysis of an ideal plano-convex focussing lens	14
12. Analytic description of the surface of an ideal focussing lens	15
13. Reduction of samples for wave-optical simulation of focussing systems	16
14. Amplitude and phase recovery of rotationally symmetric beams	17
15. Tomographic amplitude and phase recovery of vertical-cavity surface-emitting lasers using the Ambiguity function	18
D. List of recent publications	19

FOREWORD

This year we have added new technology basis for realising micro-optical and mechanical structures. Several contributions report on the properties and applications of this new type of resist. Continuing interest is in the field of micro-lenses, where we want to investigate and optimise the collimation properties. The high flexibility of mask structured ion-exchange has brought additional applications in the field of astronomy and microscopy. Jochen Bähr is currently starting a company for commercialising the results of this work. In the field of optical storage, we have addressed some fundamental question on the polarisation properties of high numeric aperture focussing lenses. Finally, Daniela Dragoman, a Humboldt visiting professor from Bucharest university, came back for experimental work on tomographic recovery of amplitude from Wigner- and Ambiguity-function, which resulted in two publications.

Karl-Heinz Brenner

Members of the chair of Optoelectronics



2	Prof. Dr. Brenner	Karl-Heinz	27 00	brenner@uni-mannheim.de
10	Dr. Bähr	Jochen	26 94	jb@oe.ti.uni-mannheim.de
7	Dragoman	Daniela	26 98	danieladragoman@yahoo.com
12	Dragoman	Mircea	26 98	mdragoman@yahoo.com
9	Ehrbächer	Ulrich	26 93	uehrbaec@oe.ti.uni-mannheim.de
8	Flammuth	Sven	26 97	flammuth@rumms.uni-mannheim.de
11	Kümmel	Peter	27 01	kuemmel@rumms.uni-mannheim.de
6	Dr. Kufner	Maria	26 92	kufner@ti.uni-mannheim.de
13	Dr. Krackhardt	Ulrich	26 92	krackhdt@rumms.uni-mannheim.de
4	Schmelcher	Thilo	26 93	tschmelcher@oe.ti.uni-mannheim.de
3	Dr. Schulze	Jens		schulze.js@t-online.de
5	Stumpfs	Wolfgang	27 02	wstumpfs@oe.ti.uni-mannheim.de
1	Volk	Sabine	27 04	office@oe.ti.uni-mannheim.de
	Walze	Günther	2698	walze@oe.ti.uni-mannheim.de

Characterization of SU-8 photoresist for alignment applications

U. W. Krackhardt, W. Stumpfs

The photoresist ‘SU-8’ has been developed by IBM in 1989 [1]. SU-8 shows singular chemical and mechanical properties: A layer thickness of up to 1000 μm is achievable. The excellent cross-linking of the resist allows for aspect ratios in the range of 25:1 (fig. 1)! There is virtually no chemical process for removing a completely processed SU-8 layer from a glass substrate. The adhesion to the glass substrate is so strong that pieces of glass are broken out when trying to mechanically remove the resist. The resist can stand temperatures of up to 230°C. Above this temperature there is no melting but ashing. The processing of SU-8 is like standard photoresist: Spin coating, UV-exposure, development, pre-, inter- and post baking. These properties make SU-8 a favorite candidate for the fabrication of alignment structures for micro-integration [2]: The lithographic process allows for highly accurate positioning. The properties provide guiding and alignment structures with strong resistance against mechanical, thermal and chemical stress. To prove the suitability of SU-8 for alignment applications the stated mechanical properties are quantified. Additionally, the accuracy of positioning and the fidelity of shape are explored.

We use SU-8/50 as a sub type of SU-8, which provides a layer thickness in the range of 500 μm (SU-8/100 allows for a thickness of about 1000 μm). The adhesion on glass is tested by a shearing experiment (fig. 2): Two glass substrates are equipped each with a SU-8 bar. Then the substrates are sheared and the force at which the bars break is monitored. The experiment is repeated with bars of different widths but otherwise constant geometry (length: 4000 μm , height 500 μm). The force is produced by a μm -screw and measured by a scales. As a result, only the structure of 250 μm width breaks within the range of the scales, namely at 2.6 N. The other bars with widths of 500 μm or 1000 μm , respectively, do not break at a force of up to 5 N.

An other vital parameter for the application of alignment structures is the shape fidelity, i.e. the change of shape due to processing. We developed a measurement procedure which provides a highly accurate observation of shrinking and swelling of the resist (fig. 3): Two glass substrates are equipped with complementary bars arranged as a V-shape and are stucked together. If there is swelling or shrinking of the bars the connecting line of the edges of the upper pair of bars forms a finite angle with respect to the edges of any of the bars (fig. 4). Measurement of angles is less subject to spatial quantization of the viewing system than direct monitoring of lateral dimensions. As result, there is a constant swelling of 2% of the bar width with a standard deviation of 0.8%. The constant deviation can be compensated for in the design process whilst the statistical error defines the reproducibility and thus the shape fidelity. As a consequence, alignment structures with widths of 125 μm provide an alignment accuracy of $\pm 1\mu\text{m}$. Experiments with an electron microscope show that the surface roughness of SU-8 is about 2 μm . Thus, the standard processing of SU-8 provides alignment accuracy of 2 μm in all 3 dimensions.

References

- [1] IBM Corp. US Patent No. 4882 245 (1989)
- [2] U.W. Krackhardt, K.-H. Brenner, „Integrated Guiding Structures for automatic Alignment of micro optical Components“, *SPIE 46. Annual Meeting, Gradient Index, Miniature, and Diffractive Optical Systems II*, Proceedings of SPIE, Vol. 4437, 91 – 98, ISSN 0277-786X/01, San Diego (2001)

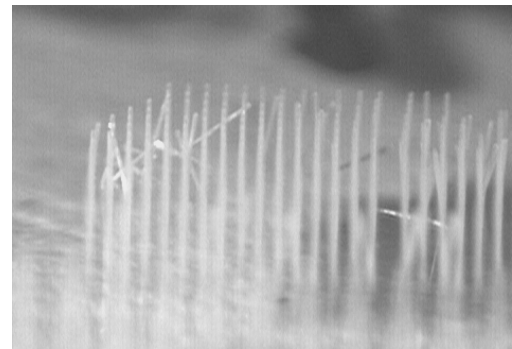


Fig. 1: Array of SU-8 cylinders with 500 μm height and $\varnothing 20\mu\text{m}$

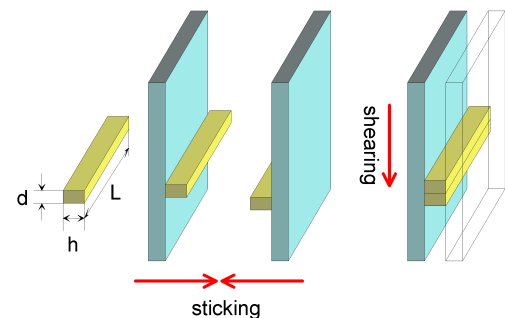


Fig. 2: Sketch of the shearing experiment

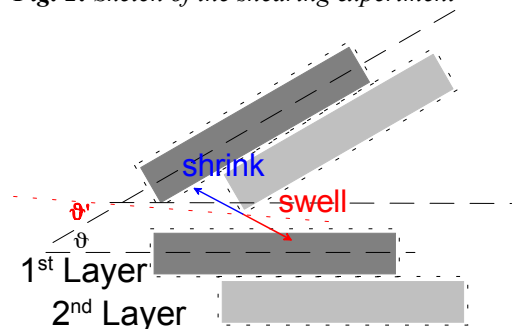


Fig. 3: Measurement scheme for shape fidelity

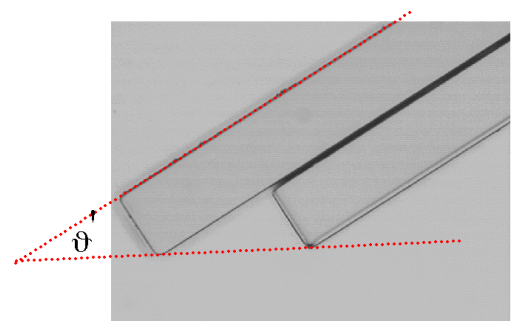


Fig. 4: Close-up of 200 μm wide bars

Micro-integration of optical modules for angle division multiplexing

S. M. Flammuth, U. W. Krackhardt

Micro-integration of the passive-optical multiplexing (MUX) and de-multiplexing modules (DeMUX) of an ADM system [1] is an essential requirement for a signal transmission system. In this report the integration of the MUX module is described, which is more challenging than the DeMUX module. Fig. 1 shows the output angle vs. input angle of a multimode step-index fiber (THORLABS, EMT-200, NA=0.39, core $\varnothing=200\mu\text{m}$) and the angular intervals for individual channels (stair-case graph). The angular width (bounding graphs) is defined by the 1/e-decay of intensity. Thus, from fig. 1, up to 11 channels may be transmitted at a cross-talk level of -10dB . The optical design of the MUX module depends on the set of input angles, the NA of the step-index fiber and the NA of the light source, e.g. a VCSEL or a single-mode fiber (fig. 2). We set up a spread sheet based design tool to obtain the NA and the positions of the micro-lens array for collimation of the individual light sources. The micro lenses show focal lengths of $630\mu\text{m}$ in air and are located at a pitch of $185\mu\text{m}$. The macro-lens is a commercial lens with NA=0.45 and $\varnothing=6\text{mm}$.

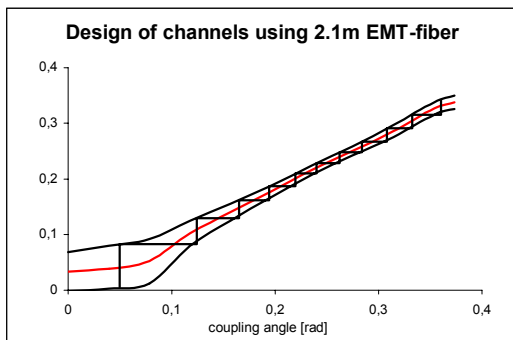


Fig. 1: Input vs. output angle of a multimode step-index fiber with 2.1m length

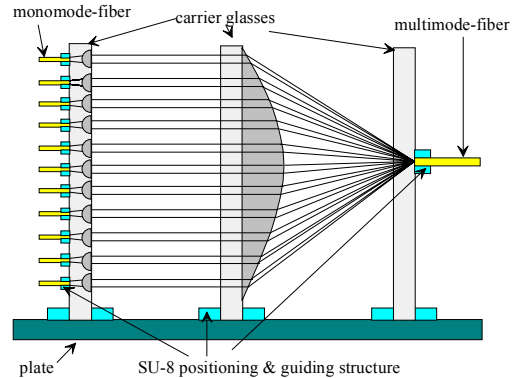


Fig. 2: MUX-module with SU-8 alignment structure

The alignment structures are realized lithographically using SU-8 photoresist [2] (Fig. 2). The single-mode fibers of NA=0.12 are mounted on the front side of a carrier glass containing the micro-lens array. The micro-lenses are realized by ion exchange in glass and are designed such that the front focal points are located at the surface of the glass carrier where the single-mode fibers are attached. The fibers are fixed by vertical fiber-holders, also realized in SU-8. The subsequent macro-lens is mounted on a different carrier glass by SU-8 structures as depicted by fig. 3. The structures are V-shaped to obtain symmetric alignment of the macro-lens which shows a circular foot print. Finally, the step-index fiber is mounted on a third carrier glass by vertical fiber-holders realized in SU-8. Each carrier glass is mounted on a common glass base plate by jamming it between SU-8 bars. The carrier glasses have a thickness of 1mm. The choice of the axial positions of the macro-lens and the step-index fiber takes into account the finite thickness of the carrier glasses. At the input of the step-index fiber this leads to an angle dependent lateral and axial displacement. However, the displacement is in the range of some few μm , which is not critical as compared to a core \varnothing of $200\mu\text{m}$.

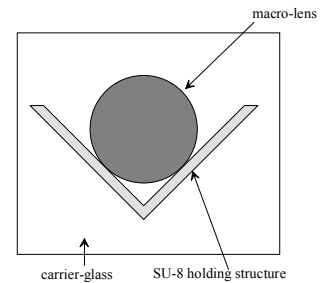


Fig. 3: V-shaped lens-holder

In our laboratories, the SU-8 process is established and we have good control of the shape fidelity of alignment structures. As an example, the V-shaped lens-holders (height $750\mu\text{m}$, width $1000\mu\text{m}$) were characterized: The location of the inner edges are measured with respect to some reference points. The target value is met up to $2\mu\text{m}$ with a standard deviation of $\sigma=8.1\mu\text{m}$ over 6 samples which leads to a vertical displacement of the macro-lens of about $5.8\mu\text{m}$. This is below 1% with respect to the lens diameter. Vertical fiber-holders are developed (Fig. 4) with fluid channels to obtain material transport during development.

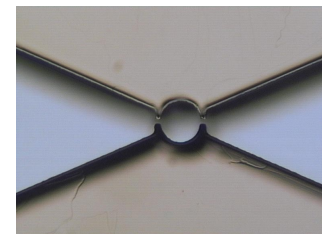


Fig. 4: SU-8 fiber-holder

References

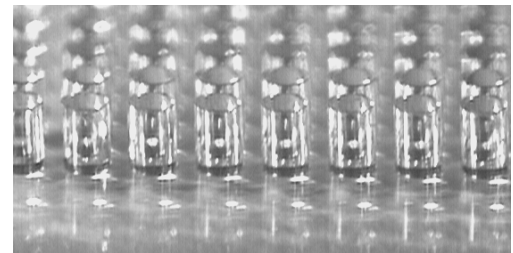
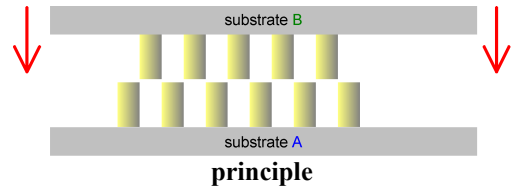
- [1] U. W. Krackhardt, R. Klug, K.-H. Brenner, „Broadband parallel fiber optical link for short distance interconnection with multi-mode fibers“, *Appl. Opt.* **39**, No. 5, 690 - 697, (2000)
- [2] U. Krackhardt, K.-H. Brenner, „Integrated Guiding Structures for automatic Alignment of micro optical Components“, *SPIE 46. Annual Meeting, Gradient Index, Miniature, and Diffractive Optical Systems II*, Proceedings of SPIE, Vol. 4437, 91 – 98, ISSN 0277-786X/01, San Diego (2001)

Integrated guiding structures for automatic alignment with μm -accuracy

U. W. Krackhardt, K.-H. Brenner

The SU-8 photoresist is an excellent tool for producing guiding and alignment structures on, e.g., glass substrates. Due to the lithographic fabrication process, high accuracy with respect to position and shape is achievable. The processed resist shows high mechanical and chemical robustness [1]. Thus, structures made in SU-8 can be used as guides for automatic alignment, i.e., for self-aligning integration techniques. We investigated different alignment strategies for various applications. When comparing alignment techniques, the figure of merit depends on robustness, mounting effort and alignment accuracy. Typically, there are two interfaces of, e.g., substrates both carrying functional structures. The substrates are equipped with guiding structures or alignment structures. The first step of any alignment procedure is realizing a mechanical contact of the interfaces. To this end, typically the interfaces are stucked together. Fig. 1 shows an example of vertical cylinders designed for interlaced insertion. However, there must be subsequent alignment steps, since insertion requires mechanical clearance which contradicts the necessity of tight fit for accurate alignment. To resolve this dilemma we propose a spiral-type alignment structure [2], where insertion and alignment function is separated by a rotation operation (fig. 2): After insertion the substrates are twisted and are thus locked. The spiral may consist of only partial paths, e.g. at the edges of the substrates, depending on the amount of clear area. The spirals may be equipped with spikes to reduce the influence of dust particles between the contact surfaces (fig. 3). A mechanical stop may be realized also in SU-8 to obtain a precise angular alignment of the substrates as well. In case of rotationally symmetric functional structures, e.g. lenses, there is no need for such a stop. Thus, any ware of the SU-8 may be compensated for by an increased rotation angle. This type of alignment by spiral structures can be applied to any interface geometry which is at least piecewise rotationally symmetric, e.g. a pair of convex/concave surfaces.

SU-8 structures are also suitable for alignment of fibers with respect to a substrate. Fig. 4 shows fiber holders which serve for horizontal coupling: A funnel is designed to facilitate fiber insertion, a square shaped channel guides the fiber with high lateral accuracy. If necessary, at the end of the channel there may be a mechanical stop, e.g. for obtaining a defined axial position of the fiber coupling interface with respect to a subsequent component.



realization in SU-8

Fig. 1: Vertical cylinders for alignment by insertion only (pitch $500\mu\text{m}$, $\varnothing 337\mu\text{m}$)

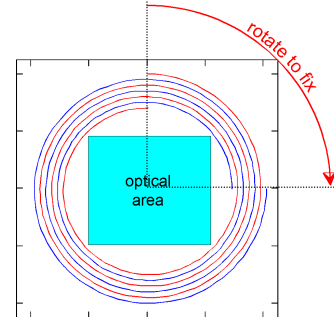


Fig. 2: Principle of alignment by spiral shaped alignment structures

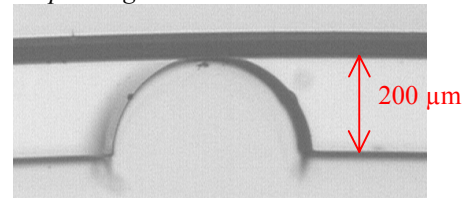
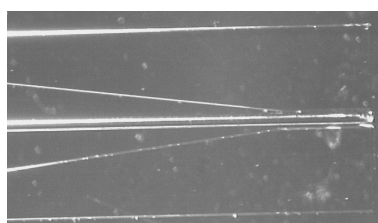
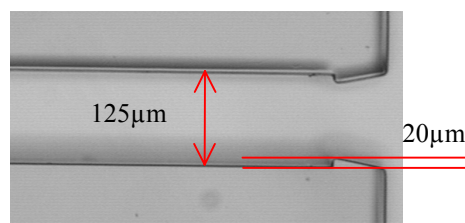


Fig. 3: Close-up of an alignment spiral with spikes realized in SU-8



a) fiber holder with inserted fiber



b) close-up of the axial stop

Fig. 4: Horizontal fiber holder realized in SU-8

References

- [1] U.W. Krackhardt, W. Stumpfs, "Characterization of SU-8 Photoresist for Alignment Applications", this report
- [2] U.W. Krackhardt, „Vorrichtung und Verfahren zur Justage in der mikrooptischen und mikromechanischen Aufbautechnik“, *patent pending* (2001)

Purely optical Sensor for absolute Measurement of Translation and Rotation

U. W. Krackhardt

Computer controlled kinematic systems require measurement of mechanical parameters such as position and orientation as a link to the real-world environment or as a feedback of remote controlled actuators. Examples are robots which assist in surgery, act in dangerous environments or perform sensitive tasks with high reproducibility. There are applications which rule out the presence of electronic devices like robotic surgery in an NMR environment where strong magnetic fields would destroy conductors or the NMR signal would be disturbed by electric currents. Also a radioactive environment would destroy electronic components.

For those kinds of applications we propose a concept we call Optical Relay Sensing (ORS): The mechanical parameters are monitored purely optically and the signals are optically transmitted to a remote system outside the hot spot which contains the electronics for finally processing the signals. To reduce wiring, angle division multiplexing (ADM) [1] as a purely optical multiplexing technique is applied.

The basic idea of a sensor is the combination of common sensing principles with fiber based signal transmission such that there is no need for electronic devices at the location of sensing. Here we discuss sensors for incremental and absolute measurement of translation and rotation. The kinematic parameter is monitored by code plates. The code plate is illuminated and the reflected or transmitted optical power is modulated while the kinematic parameter changes (fig. 1). Both illumination and detection is realized by fibers. Commercial ferrules are used to reduce costs while maintaining high position accuracy and easy mounting. We use MT-O ferrules with the metallic guiding pin removed, resulting in a metal-free fiber holder. Micro lenses fabricated by ion exchange in glass are applied to minimize cross-talk and noise. The glass substrate is mounted on the ferrule by alignment guides realized in SU-8 photoresist [2].

For incremental measurement a regular grating is sufficient to count the ties while the code plate moves. Commonly, for the detection of direction two code tracks with a relative phase offset of 90° are used. Fig. 1 sketches a relative sensor with the reflective code plate being moved perpendicularly to the drawing plane. Absolute measurements require absolute codes, e.g. Gray Code. Absolute code plates consist of multiple code tracks which require a multi-channel signal transmission. Using Gray Code, an absolute code plate for, say, 2^{12} subdivisions requires 12 code tracks. For this type of sensors all 12 fibers of an MT-O ferrule are used for detection. A separate fiber is used for illumination (fig. 2). For optimization of the optical efficiency a system of cylindrical lenses is used to generate a line-shaped intensity distribution impinging on the micro-lens array (fig. 3). The optical components are stacked using automatic alignment provided by suitable guiding structures realized in SU-8 photoresist [2]. Also, the ferrules for the illumination and detection fibers are mounted using SU-8 guiding structures. As a result, the sensor concept provides mechanical standard interfaces and can be mounted even by operators with no optical skill. The sensor principle can be applied to measurement of translation (linear code plates) or rotation (circular code plates). In general, any quantity which can be mechanically transformed to a translation or a rotation can be monitored by this type of sensor. Examples are force sensors transforming force to translation via Hook's law of elastic deformation or pressure sensors transforming pressure to dilatation of an elastic surface and measuring the change of shape by observation of displacement, i.e. by a translation sensor.

References

- [1] U. W. Krackhardt, R. Klug, K.-H. Brenner, „Broadband parallel fiber optical link for short distance interconnection with multi-mode fibers“, Appl. Opt. **39**, No. 5, 690 - 697, (2000)
- [2] U. W. Krackhardt, „Integrated Guiding Structures for Automatic Alignment with μm -Accuracy“, this report

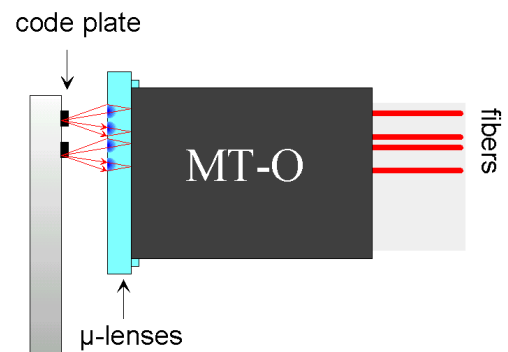


Fig. 1: Sketch of a relative sensor with two code tracks using a commercial ferrule

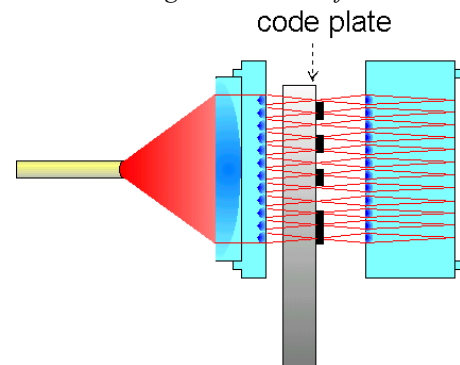


Fig. 2: Sketch of an absolute sensor with illumination (left) and detection (right) set-up

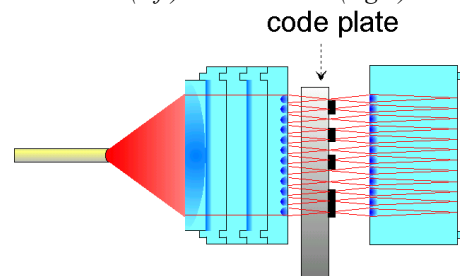


Fig. 3: Like fig. 2 but with a system of cylindrical lenses for adapted illumination

Investigation of collimation properties of microlenses

U. Ehrbächer, K.-H. Brenner, J. Bähr

In the field of optical switching, free space optical cross-connects have become a viable alternative to waveguide solutions. For such setups the use of collimated laser beams is necessary. When using micro-optics and lasers, the wave aspects of light have to be taken into account. The effects to be considered are:

- Small beam radii of the lasers cause strong beam divergence
- Small apertures cause diffraction and thus also strong beam divergence
- The beam radius depends strongly on the propagation distance

This leads to a trade off between these effects when considering the power efficiency of a system using micro-optics for collimating lasers.

The investigation of this problem has to lead to a merit function to judge optical free space interconnects with regards to input beam width, aperture sizes and possible propagation distances. As a first step, the light propagation through such a system of microlenses was simulated numerically. At the first aperture with radius a , an initial Gaussian beam distribution $u(n \cdot \delta r, m \cdot \delta r, 0)$ is given with radius βa and initial power

$$P_0 = \sum_{n=-\frac{N}{2}}^{\frac{N}{2}} \sum_{m=-\frac{M}{2}}^{\frac{M}{2}} |u(n \cdot \delta r, m \cdot \delta r)|^2 \quad (1)$$

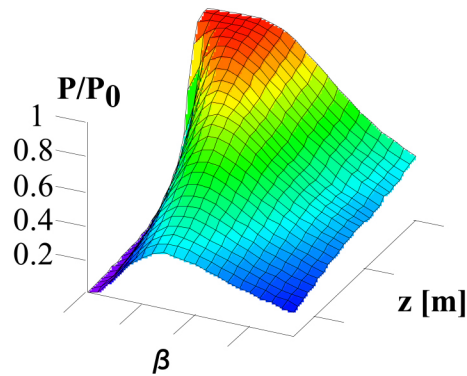


Fig. 1: Simulated power efficiency of an ideal lens (z .range: 0 - 1.3m, β range 0.1 - 2.4)

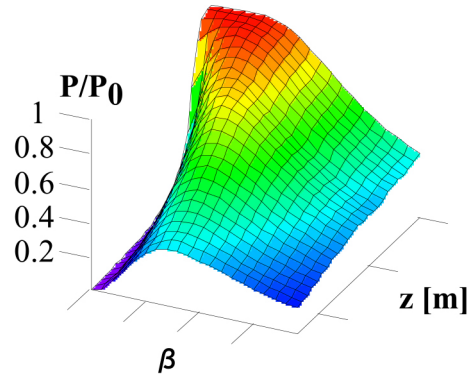


Fig. 2: Simulated power efficiency of a planar GRIN microlens (same axes range as in Fig. 1)

This initial beam distribution can also include a phase function due to propagation prior to the first aperture or due to lens aberrations. This beam distribution is truncated and propagated over a distance z , where the distribution $u(n \cdot \delta r, m \cdot \delta r, z)$ is truncated by a second aperture with radius a and the output power P_{out} is calculated according to e.q. 1. The ratio of P_0 and P_{out} gives the merit function mentioned above. Fig. (1) and (2) show the simulation of an ideal and a planar GRIN microlens, fabricated by J. Bähr, respectively (both with same radius of $280 \mu m$) over a z range of 0 - 1.3m and a beam/aperture ratio β of 0.1 - 2.4. Fig. (3) shows the difference in power efficiency of the two lenses, indicating how close the planar GRIN microlens is to an ideal lens.

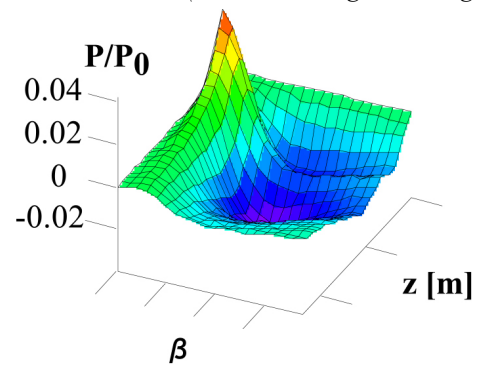


Fig. 3: Difference in simulated power efficiency of ideal and planar GRIN microlens (same axes range as in Fig. 1)

Parallel method for testing an array of micro lenses

J. Bähr, K.-H. Brenner, U.W. Krackhardt

Most of the common methods for characterization of micro lens arrays perform sequential measurements of individual lens parameters, which makes the characterization of lens arrays expensive and time consuming. For rapid quality control, often only a subset of the lenses is considered thus, some local errors might be left undetected.

To attain accurate and rapid quality control we made an investigation on the characteristics of lens errors. In principle, errors of lens arrays can be classified as local or global variations. For measurement of global parameters it is basically sufficient to evaluate only a single representative lens within the array. However, detection of local variations commonly require a sequential measurement of each individual lens.

Local variations result in aberrations, which can be discriminated to be symmetric or non symmetric. The symmetric aberrations lead to a loss of intensity in the spot center. The non symmetric aberrations lead to a lateral focal shift. So by analyzing the spot intensity and the focal positions the local variations can be detected. This detection can be performed in parallel by monitoring the spots with a CCD camera.

The photolithographic process of the MSI technique provides high precision of the mask structure. The properties of the micro lenses on the substrate depend on duration and temperature of the exchange process, on the strength of the electrical field and in particular on the design of the mask structure. All these parameters affect the whole substrate and determine the global lens parameters. These global parameters are checked by measuring the focal length and the wave aberrations in an interferometer.

Local variations of the lens parameters are caused by local defects of the mask structure, i.e. scratches or pinholes within the titanium layer. These defects result in small non-symmetric aberrations of the affected micro lenses and lead to lateral focal shifts. As a consequence, the proposed method can be applied to lens arrays fabricated by the MSI technique.

The focal positions are analyzed by measuring the center of gravity of the intensity distribution in the focal plane for plane wave illumination. To compare the focal positions with the scheduled values, different approaches are possible: For non periodic arrays, the measured positions can be compared with vector data of the scheduled values. An alternative method is to use a reference pattern on a separate substrate, which has to be located in the focal plane. In the latter case two separate measurements are required. In addition to these methods, a periodic arrangement of foci, for example cartesian or hexagonal arrangements, can be investigated by Fourier analysis. The analyzed periodicity can be compared to scheduled data.

Estimation of sensitivity

For simplification we consider a phase ramp with a constant tilt angle α over the aperture of one lens. For a small angle α or a small height of the prism h_{prism} , respectively, the lateral focal shift Δr_{shift} can be written as

$$\tan \alpha = \frac{h_{prism}}{d_{lens}} = \frac{\Delta r_{shift}}{f} \Rightarrow \Delta r_{shift} \cong \frac{h_{prism}}{2 \cdot N.A.} \quad (6)$$

The sub-pixel resolution of a standard CCD camera (8bit) can be estimated as 1/10 – 1/20 of a pixel, which typically allows a lateral resolution of 0.5-1 micron. Thus, assuming a prism height of $h_{prism} = \lambda/4$, according to eq. 6, we can measure lenses with numerical apertures of up to N.A. of 0.16 with this method.

References

[1] J. Bähr, U. Krackhardt, K.-H. Brenner „Fabrication and Testing of planar Micro Lens Arrays by Ion Exchange Technique in Glass“, SPIE 46. Annual Meeting, Workshop on Microlens Measurement Standardization, San Diego, USA, to appear in SPIE Proceedings (2001)

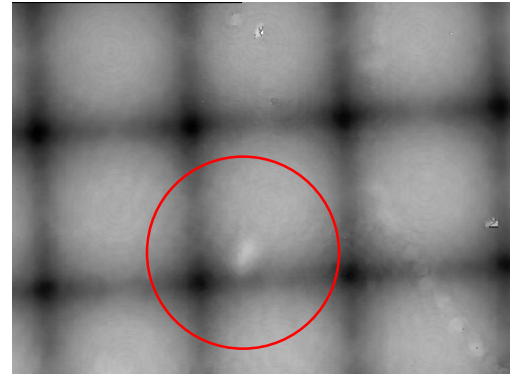


Fig. 1: phase distribution of local defect within an array of square shaped microlenses

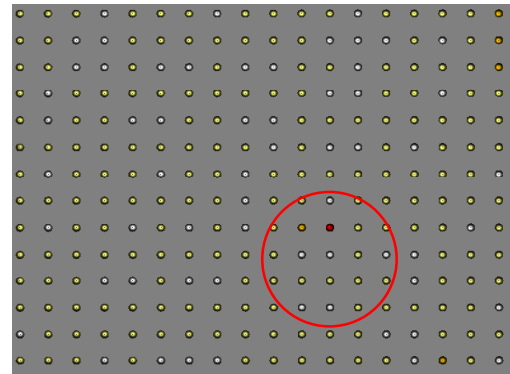


Fig. 2: detection of the defect shown in fig. 1 by investigation of the positions of the spots (marked by circle)

Alignment through a thick substrate

J. Bähr, J. Bewersdorf* (*J. Bewersdorf: MPI for Biophysical Chemistry, Göttingen)

We report the alignment procedure for two layers of structures over a distance of 7.5 mm with an accuracy better than 2 μm . The geometry of the alignment procedure is demonstrated in fig. 1.

The alignment is performed in two steps according to fig. 2 and 3. Within the first wafer micro lenses are integrated; the foci of the lenses are designed to lie on the back side of the substrate. The micro lenses are fabricated with the silver-sodium ion exchange. The masks for the lens fabrication process is realized in the same photolithographic process as that of structure 1, thus the lens positions are accurate.

In the first alignment step the lateral positions of the micro lenses on the front side are transferred into a photo resist layer on the backside by perpendicular plane wave illumination. The structure in the photo resist now is in the same z-position as the structure of the second wafer. Thus the second alignment step can be performed under a microscope with high accuracy.

The most difficult part of the procedure is to ensure the exact angle of the incident light in the first alignment step. A deviation of the angle leads to a shift of the foci on the back side of the wafer according to

$$\Delta x = f \cdot \tan(\vartheta)$$

There f must be taken as the focal length in glass, which differs from the focal length in air.

For an optimization of the accuracy of the incident angle, we performed a double exposure, where we shifted and turned the wafer within the stage as demonstrated in fig. 2. For a deviation of the perpendicular direction now two separate spots are obtained. The ideal spot position is represented by the center of gravity of both spots.

In our experiment we obtained an alignment accuracy of better than 2 microns over a thickness of 7.5 mm.

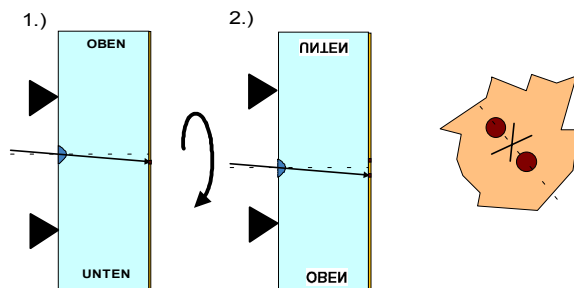


Fig. 4: double exposure of turned sample. The center of gravity marks the ideal spot position.

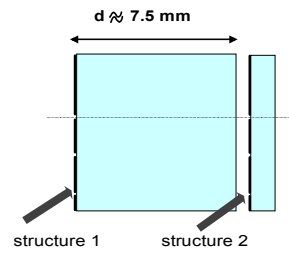


Fig. 1: geometry of the alignment: the layers both are structured on their left side

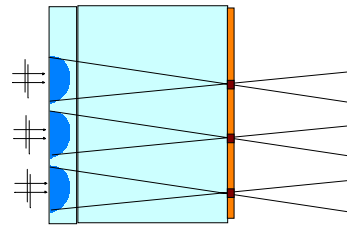


Fig. 2: step 1: transfer of the positions to a photo resist layer on the back side of substrate 1 using micro lenses

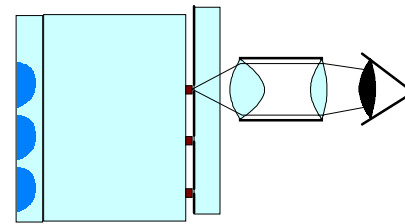


Fig. 3: step 2 passive alignment of the second layer to the structured photo resist under microscope

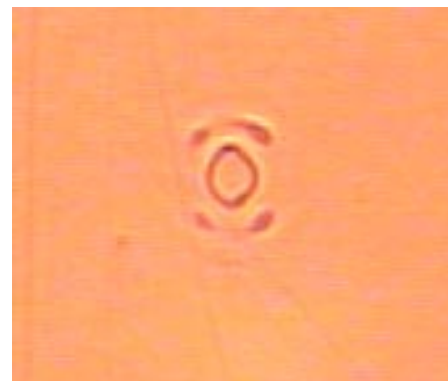


Fig. 5: pattern after double exposure. The spot diameters are 5 μm . The shift of the spots is less than 2 micron.

Phase screens for astronomical applications

*J. Bähr, D. Butler**(*Max-Planck-Institut für Astronomie, Königstuhl 17, 69117 Heidelberg*)

We report the realization of prototypes of phase screens for simulation of atmospheric turbulence using the MSI technique. The investigation of far away star systems by earth based astronomy suffers from turbulence of the atmosphere. Thus the resolution even of large telescopes is strongly limited. To overcome these problems, in a project named MCAO (Multi Conjugated Adaptive Optics) telescopes are to be upgraded by adaptive optical systems, which are able to measure the atmospheric perturbation with wave front sensing tools (e.g. Shack-Hartmann sensors) and to correct them online using a moveable mirror in a closed loop arrangement.

For testing of different approaches of adaptive optical systems the European Southern Observatory (ESO) in Garching and the Max-Planck Institute of Astronomy (MPIA) in Heidelberg are working on a low cost test system for the physical generation of atmosphere turbulence in the lab. Therefore phase screens were realized, which represent a down scaled static copy of the typical density distribution (Kolmogorov-distribution) and thus the refractive turbulence of the atmosphere. For approximation of the layered structure of the atmosphere in z-direction a series of different consecutive phase screens were applied where a certain layer is simulated by a phase screen with a distinct phase distribution. Dynamic properties of the atmosphere (i.e. wind) can be simulated by movement of the single screens. According to the calculation of ESO and MPIA for simulation of atmospheric properties the Kolmogorov statistic at a certain phase height (PV=10.2 waves at $\lambda=633\text{nm}$) has to be ensured.

For realization the MSI technique is applied. The input data plane was sampled in a grid with $80\ \mu\text{m}$ pitch. The phase value of each sampling point represents the average value within a cell of $80 \times 80\ \mu\text{m}$ size. The exchange mask consists of $n \times n$ elementary cells (fig. 1) where the aperture density in each cell provides an ion migration in the glass to attain the demanded average phase value homogeneously within each elementary cell. After a subsequent post heating step a continuous 2D phase distribution is obtained.

To proof the quality of the reproduction of certain input phase data a set of phase ramps with different phase gradients at the demanded PV value has been performed. Figure 2 demonstrates the linearity and therefore the performance of the MSI technique to realize a certain phase distribution.

To ensure the quality of the MSI technique in first tests the power spectrum of the test screens was measured and compared to the input data. Fig. 1 demonstrates the good consistence. The power in the phase fluctuation spectrum varies as $f^{-11/3}$ where f is spatial frequency. The value $-11/3$ is the value expected for our target, a Kolmogorov spectrum.

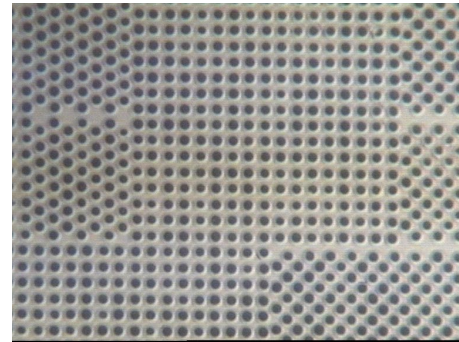


Fig. 1: mask of 4 x 3 elementary cells

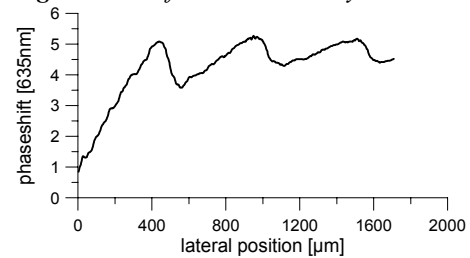


Fig. 2: scan of a phase distribution consisting of several linear ramps

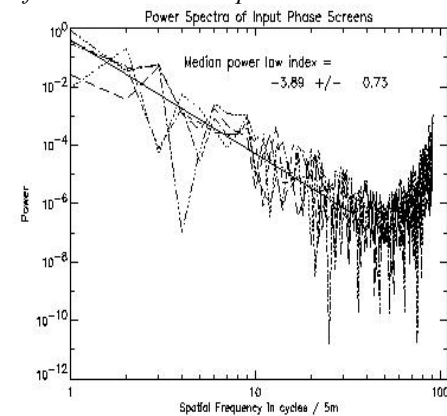


Fig. 3: power spectrum of computer generated phase screens

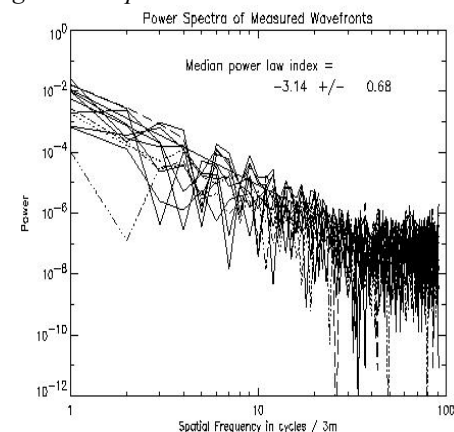


Fig. 4: measured power spectrum from phase screens realized by the MSI technique

Improvement of power efficiency by two-dimensional beam shaping

K.-H. Brenner

Beam shaping is used to transform a given intensity distribution into a different, desired intensity distribution. The conversion of a Gaussian intensity distribution into a uniform profile is well established for the case of one-dimensional or rotationally symmetric distributions. Applications of beam shaping are typically in the area of high power laser operations, where the Gaussian beam shape leads to an inefficient usage of the available laser power due to loss at the focusing lens.

In the application described here, the transformation of a non-symmetric Gaussian beam with intensity

$$I_1(r, \varphi) = e^{-2r^2 \left[\left(\frac{\cos \varphi}{\sigma_x} \right)^2 + \left(\frac{\sin \varphi}{\sigma_y} \right)^2 \right]} = e^{-2r^2 A(\varphi)}$$

from a semiconductor laser into a rotationally symmetric homogeneous flat top distribution is used to maximise the power transfer to an optical disk and to minimise the spot diameter at the disk surface. In order to achieve a diffraction limited focal spot, the amplitude in the plane of the focusing lens has to be constant. Conventionally this requirement is satisfied by using only the inner fraction of the Gaussian beam profile. If the aperture radius, for example is 0.3σ , the rim intensity, i.e. the intensity at the aperture edge drops to 84% and the transmitted power is approximately 26 % of the total power. By beam shaping, the amplitude drop can be removed, leading to a minimum focal spot size. At the same time, the efficiency can be increased to almost 100 %.

The front-surface design consists of three steps. The first is to find a mapping $\vec{r}_2(\vec{r}_1)$, which maps every point \vec{r}_1 on the front-surface to a point \vec{r}_2 on the back surface. This is achieved by applying the law of power conservation for the rotationally symmetric case:

$$\int_0^{r_1} I_1(r) \cdot r \cdot dr = \int_0^{r_2} I_2(r) \cdot r \cdot dr$$

The second step is a linear transformation of the mapping, to respect the asymmetric shape of the laser. The third step, the calculation of the front surface, is based on the vectorial law of refraction, described in the next contribution in this annual report. In order to compute the surface shape from the surface normals, a path integral has to be applied. Ideally, this path integral should be independent of the chosen path. This requirement, however, cannot be met for all mappings. For the problem, described here, the deviation from path independence is small, but not zero. Fig. 1 shows the height distribution of the front surface, calculated with this method. In order to correct for both, the intensity and the phase, a second element, which changes the ray direction is necessary. The design for the back-surface is based also based on the vectorial law of refraction and on the equal path-length condition. Fig. 2 shows the x- and y-view of the ray path through the system. In this case, the back-surface was designed to generate a divergent spherical wave at the element output.

Because of this modification of the ray density, refractive beam shaping is not limited to coherent light. Moreover, a modification of local ray density is not limited to the use of light at all. For any beam of particles which propagate along straight lines in free space, modification of ray density can be used for beam shaping.

References

[1] K.-H. Brenner, "Element zur kombinierten Symmetrisierung und Homogenisierung eines Strahlenbündels", German Patent, Filing No. 10121747.1 (2001)

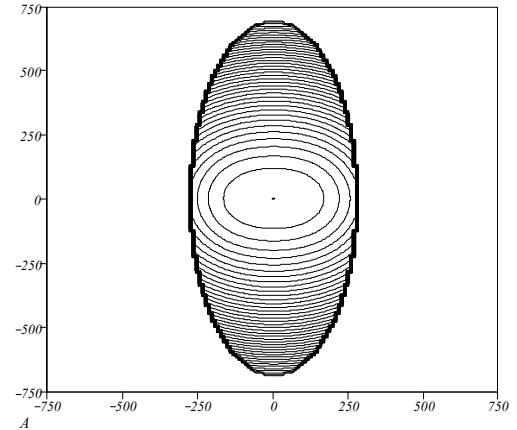


Fig. 1: Height distribution of the front surface. The visible area is 1,5 mm × 1,5 mm

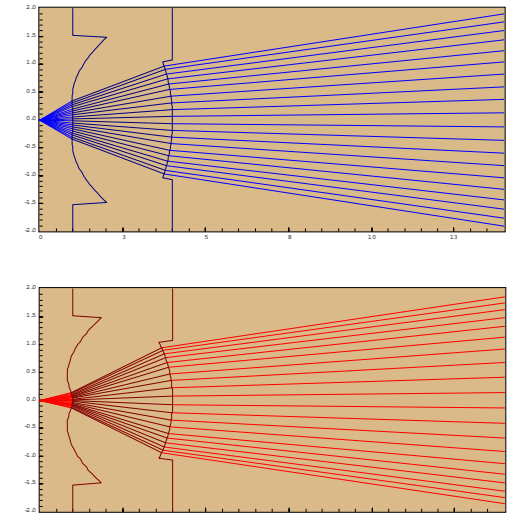


Fig. 2: Ray trace of the transformation of an asymmetric laser intensity to a homogeneous, symmetric intensity by beam shaping. top: x-view, bottom: y-view.

Calculation of surfaces from ray directions

K.-H. Brenner

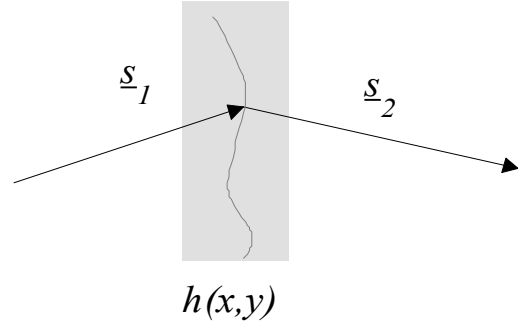
In geometrical optical design, it is a frequent situation, that the ray directions before and after the surface are given, but the shape of the surface, which transforms the incoming ray into the outgoing one, is unknown. The law, which describes this situation mathematically, is the law of refraction:

$$n_2 \vec{s}_2 = n_1 \vec{s}_1 + \vec{N} \left(\sqrt{n_2^2 - n_1^2 + (n_1 \vec{s}_1 \cdot \vec{N})^2} - n_1 \vec{s}_1 \cdot \vec{N} \right) \quad (1)$$

Here \vec{s}_1 and \vec{s}_2 are the unit vectors before and behind the surface and \vec{N} is the surface normal. The relation between the surface normal and the surface height distribution $h(x, y)$ is given by:

$$\vec{N}(x, y) = \frac{1}{\sqrt{1 + h_x^2 + h_y^2}} \begin{pmatrix} -h_x \\ -h_y \\ 1 \end{pmatrix}$$

where h_x and h_y are the partial derivatives of the surface height. Thus we can recover the normalization factor from the z-component of the normal vector and $h(x, y)$ can be determined subsequently by a path integral.



The problem is to solve equation 1 for the normal vector.

At first glance, this seems difficult, since the normal vector appears three times in this equation. The essence of this report is to describe, that two simple assumptions are sufficient, to solve for the normal vector in eq. 1. First, we rewrite eq. 1 as

$$n_2 \vec{s}_2 - n_1 \vec{s}_1 = \vec{N} \cdot f(n_1, n_2, \vec{s}_1, \vec{N}) \quad (2)$$

The assumptions are, that $|\vec{N}| = 1$ and that f is real. These assumptions are in fact trivial, but they allows us to state the equality:

$$|\vec{N}| = \left| \frac{n_2 \vec{s}_2 - n_1 \vec{s}_1}{f} \right| = 1$$

Thus, we can determine the magnitude of f :

$$|f| = |n_2 \vec{s}_2 - n_1 \vec{s}_1|.$$

Using eq. 2, we can state, that

$$\vec{N} = \frac{n_2 \vec{s}_2 - n_1 \vec{s}_1}{f} = \pm \frac{n_2 \vec{s}_2 - n_1 \vec{s}_1}{|n_2 \vec{s}_2 - n_1 \vec{s}_1|}$$

In this way, we have determined the vector normal vector up to an unknown sign. The sign of the normal vector is usually of no concern, since both, $\pm \vec{N}$ are valid normal vectors, if the surface is not closed. In the case of vectorial refraction, the sign of \vec{N} , however, is important, since eq. 1 is not symmetric with respect to a sign change of the normal vector. In the vectorial refraction law, the assumption is that the normal points in the direction of the second medium. Therefore the sign of the Normal vector can be determined uniquely from the scalar product $\vec{s}_2 \cdot \vec{N}$ which must be positive and the surface normal is thus also determined uniquely.

Polarisation analysis of an ideal plano-convex focussing lens

K.-H. Brenner

We call a focussing lens 'ideal', if it focuses a perfectly plane wave into a perfect spot. In a more strict sense, we require that all the rays with a unit direction vector $\vec{s} = \vec{e}_z$ are focussed into one geometric spot, after being refracted by the front- and back-surface according to the vectorial law of refraction

$$\vec{t}_2 = \vec{t}_1 + \vec{N} \left(\sqrt{n_2^2 - n_1^2 + (\vec{t}_1 \cdot \vec{N})^2} - \vec{t}_1 \cdot \vec{N} \right) \quad (1)$$

Here $\vec{t}_j = n_j \vec{s}_j$ are the unit direction vectors before and behind a surface, weighted with the corresponding refractive index and \vec{N} is the surface normal. For a focussing lens with a very high numerical aperture NA, polarisation effects need to be considered. In this report, we have shown, that for the case of a planar back surface, i.e. a plano-convex lens, the polarisation state of the electric field vector behind the back surface can be computed analytically, without determining the exact shape of the front surface. Using these assumptions, the weighted direction vector inside the lens, as well as the normal of the front-surface can be computed from the weighted direction vector \vec{t}_2 behind the lens by:

$$\vec{t}_1 = \vec{t}_2 - \vec{e}_z (t_{2z} - t_{1z}) \quad \text{with } t_{1z} = \sqrt{t_{2z}^2 + n^2 - 1}, \quad \text{and } \vec{N} = N_z \left(\frac{\vec{t}_1 - \vec{t}_0}{t_{1z} - 1} \right) \quad \text{with } N_z = \frac{t_{1z} - 1}{\sqrt{n^2 - 2t_{1z} + 1}}$$

With these parameters, the electric field inside the lens can be determined analytically from the electric field \vec{E}_0 before the lens, by decomposing the field into the s- and p- components and using the Fresnel coefficients of transmission:

$$\vec{E}_1 = \left(\left(\frac{\vec{E}_0 \cdot \vec{t}_0 \times \vec{N}}{|\vec{t}_0 \times \vec{N}|} \right) \frac{2N_z}{N_z + \vec{t}_1 \cdot \vec{N}} \right) \frac{\vec{t}_0 \times \vec{N}}{|\vec{t}_0 \times \vec{N}|} + \left(\left(\frac{\vec{E}_0 \cdot \vec{t}_0 \times (\vec{t}_0 \times \vec{N})}{|\vec{t}_0 \times (\vec{t}_0 \times \vec{N})|} \right) \frac{2N_z}{nN_z + \vec{t}_1 \cdot \vec{N} / n} \right) \frac{\vec{t}_1 \times (\vec{t}_0 \times \vec{N})}{|\vec{t}_1 \times (\vec{t}_0 \times \vec{N})|}$$

In the same way, the electric field behind the lens can be determined analytically:

$$\vec{E}_2 = \left(\left(\frac{\vec{E}_1 \cdot \vec{t}_1 \times \vec{e}_z}{|\vec{t}_1 \times \vec{e}_z|} \right) \frac{2t_{1z}}{t_{1z} + t_{2z}} \right) \frac{\vec{t}_1 \times \vec{e}_z}{|\vec{t}_1 \times \vec{e}_z|} + \left(\left(\frac{\vec{E}_1 \cdot \vec{t}_1 \times (\vec{t}_1 \times \vec{e}_z)}{|\vec{t}_1 \times (\vec{t}_1 \times \vec{e}_z)|} \right) \frac{2t_{1z}}{t_{1z} / n + n t_{2z}} \right) \frac{\vec{t}_2 \times (\vec{t}_1 \times \vec{e}_z)}{|\vec{t}_2 \times (\vec{t}_1 \times \vec{e}_z)|}$$

Since the Fresnel coefficients also account for reflection losses, this analytic result is accurate except for multiple reflections inside the lens. Also it is interesting, that the exact shape of the front surface is not necessary for this description. Fig. 2 shows the results for a NA=0.95 lens and x-polarization at the input. The amplitude drops down to 0.25 at the top edge and the polarization direction rotates toward the edges.

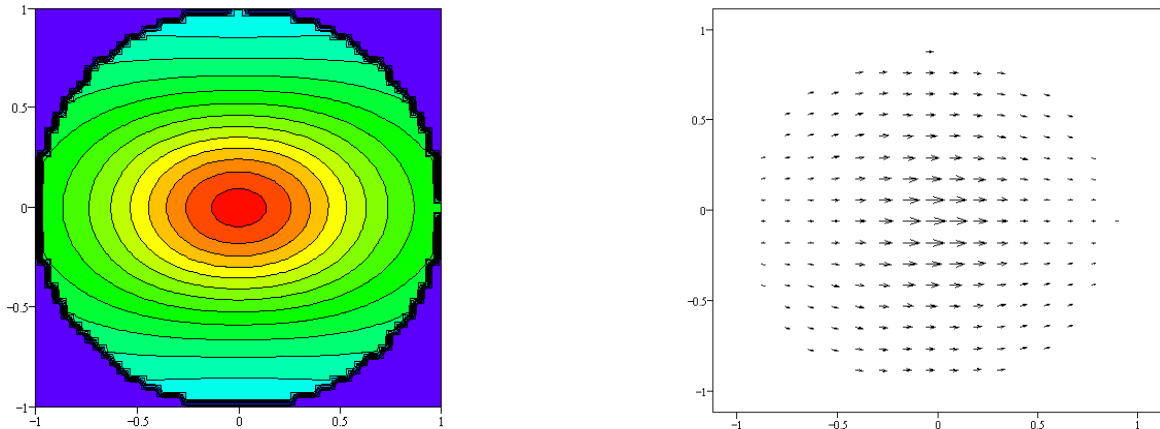


Fig. 2: Electric field behind the focussing lens, using an x-polarised plane wave as input distribution. left side: amplitude in steps of 0.05, max. = 0.92; right side: direction of polarisation

Analytic description of the surface of an ideal focussing lens

K.-H. Brenner

The design of ideal focussing lenses is usually performed with ray trace software, by modelling the surfaces with a polynomial and performing an optimisation on the coefficients. There are, however, also cases where an analytic description of the surface is needed. Examples for this are situations, where the interdependencies of various parameters are of interest. A simple example might be the dependence of surface sag on the numeric aperture. In this report, we have restricted our treatment to the case of ideal plano-convex lenses and we have developed a fully analytical description of the front surface.

The geometry of the focussing situation is depicted in fig. 1. The lateral position of an incoming ray is x and z denotes the longitudinal position of the surface, assuming $z = 0$ on the optical axis. The lens thickness is D and w is the working distance, i.e the distance from the back surface to the focal point. The description presented here, uses the numeric aperture NA , the lens radius R , the refractive index n and the x-component of the direction vector \vec{s} behind the lens as the describing parameters. Using the equal path-length condition, the lens thickness and the working distance can be expressed as:

$$w = \frac{R}{NA} \sqrt{1 - NA^2} \quad (1)$$

$$D = \frac{1}{n-1} \frac{R}{NA} \left(1 - \sqrt{1 - NA^2}\right) \quad (2)$$

The lateral position x can then be expressed as a function of the z -position and $s = s_x$:

$$x(s) = s \left(\frac{D - z(s)}{\sqrt{n^2 - s^2}} + \frac{w}{\sqrt{1 - s^2}} \right) \quad (3)$$

The surface height $z(s)$ can be expressed as a function of s , D and w :

$$z(s) = \frac{nD \left(1 - \frac{n}{\sqrt{n^2 - s^2}}\right) + w \left(1 - \frac{1}{\sqrt{1 - s^2}}\right)}{1 - \frac{n^2}{\sqrt{n^2 - s^2}}} \quad (4)$$

The description, presented here is a parametric representation of x and z on the x-component of direction vector, which is e.g. useful for the Debye formalism of diffraction, where the pupil is parameterized by the direction vector \vec{s} . Fig. 2 shows the case $R=1$, $n=1.5$ and $NA=0.6$. The thickness D in this case is 0.67 and the working distance w is 1.33.

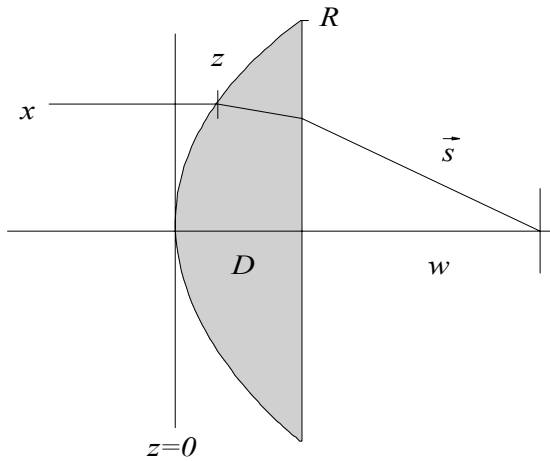


Fig. 1: Geometry of the ideal focussing lens

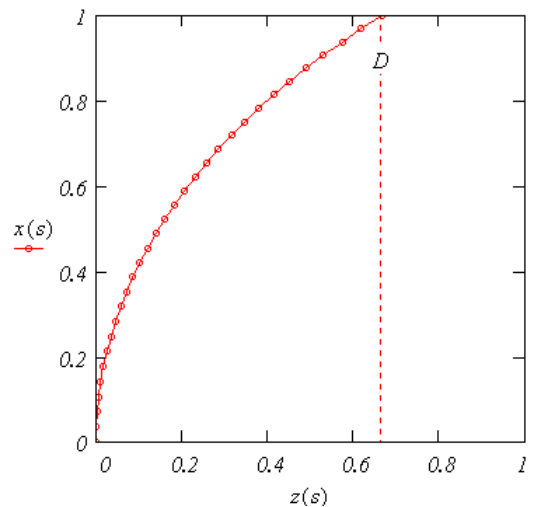


Fig. 2: Front surface, calculated from eq. 3,4

Reduction of samples for wave-optical simulation of focussing systems

K.-H. Brenner

In order to investigate diffraction properties of optical systems, wave optical simulations are required. In the realm of micro-optics, wave optical calculations can be implemented without problems, since the dimensions and hence the number of samples are manageable by today's computers. For the case of macro-optical systems, a wave-optical simulation is only possible for extremely low numeric apertures. To illustrate this, we consider the case of a focussing lens with 3mm diameter, $\lambda = 400$ nm and a numerical aperture of 0.85. The phase factor of the focussing lens has a spatial frequency of:

$$v(r) = \frac{k_0 r}{2\pi\sqrt{f^2 + r^2}} \quad \text{and hence, } v_{\max} = \frac{k_0}{2\pi} NA$$

Using the Nyquist-criterion, the minimum number of samples, required for the lens is therefore

$$N_L = \frac{k_0 R \cdot NA}{\pi}$$

With the even moderate numbers, stated above, the required number of samples is 12590 in one dimension. It is straight forward to see, that a two-dimensional treatment with single precision requires already 1.3 GB to store one array. Since the extent of the focal plane is very small, it must be possible to reduce the necessary number of samples. In this report, we describe a method, which is based on the idea, to combine the phase function of the lens with the propagation phase factor by subtracting a quadratic phase factor, which minimises the spatial frequency of the lens phase. We describe the amplitude transmission of the reduced lens by:

$$t_L(r) = \begin{cases} e^{ik_0\left(f - \sqrt{f^2 + r^2} + \frac{r^2}{2f_0}\right)} & |r| < R \\ 0 & \text{else} \end{cases} \quad \text{resulting in } v(r) = \frac{k_0 r}{2\pi} \left(\frac{1}{f_0} - \frac{1}{\sqrt{f^2 + r^2}} \right)$$

with the focal length f_0 of the reduction lens chosen to minimise the maximum of $v(r)$. With this addition, the non-paraxial Rayleigh-Sommerfeld diffraction integral:

$$u_z(r) = \iint t_l(r') e^{ik_0 \frac{r'^2}{2f_0}} e^{ikz\sqrt{1-\lambda^2\rho'^2}} e^{-2\pi i\rho(r'-r)} d^2r' d^2\rho$$

can be expressed as $u_z(r) = C \cdot \int W(r'') e^{ik_0 \frac{r''^2}{2f_0}} e^{ik_0 z\sqrt{1-(r''/f_0)^2}} e^{-i\frac{k_0 r'' r}{f_0}} d^2r''$, with $C = -e^{-\frac{\pi}{4}} \sqrt{\frac{k_0}{2\pi f_0}}$,

with $W(r'') = \int \tilde{v}(\rho') e^{i2\pi^2 \frac{f_0}{k_0} \rho'^2} e^{2\pi i\rho' r'} d^2\rho'$

and $\tilde{v}(\rho') = \int t_L(r') e^{-2\pi i\rho' r'} d^2r'$.

The treatment of a focussing lens is thus reduced to three Fourier transforms. Fig. 1 shows the case of a 1.2 mm diameter lens with NA 0.06, yielding a reduction factor of 45. Conventionally (top), 360 samples are necessary. Using 1024 samples, we have an oversampling factor of 3. With the reduction method (bottom), only 8 samples are necessary, allowing us an oversampling factor of 16 using 128 samples. An oversampling factor of 1 corresponds to one sample per peak.

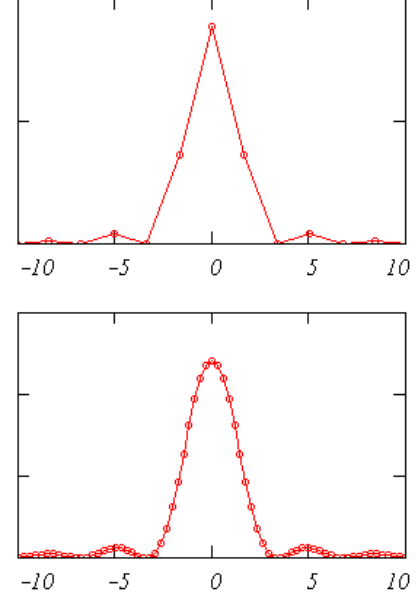


Fig. 1: Comparison of conventional and reduced method. Top: 1024 samples, oversampling factor 3; reduced method, bottom: 128 samples, oversampling 16.

Amplitude and phase recovery of rotationally symmetric beams

D. Dragoman, M. Dragoman, K.-H. Brenner

The amplitude and phase recovery of optical fields is a significant issue in many areas of optics and opto-electronics, especially in applications such as adaptive optics or advanced optical data processing. Up to now wavefront recovery from tomographic measurements was done using an algorithm based on the Wigner distribution function (WDF) for one-dimensional (1D) optical beams or optical pulses. This was possible since for 1D beams or optical pulses the WDF is two-dimensional (2D). For a general 2D optical beam $\varphi(x, y)$, however, the corresponding phase-space distribution is four-dimensional (4D), and thus only 2D slices or projections of them can be optically generated. In this report, we demonstrate that, if the 2D beam is rotationally symmetric, the 4D WDF can be fully recovered from the 2D WDF of its 1D approximation. In ref. 1 we have demonstrated that the value of the WDF of a rotationally symmetric beam can be calculated, for any set of variables, as an integral transform of the WDF of $\varphi(x, y)$. For the measurement, using the setup in fig. 1, we generate in the CCD plane the complex amplitude

$$\Psi(x, y) = \varphi(x \cos \alpha + y \sin \alpha) \exp[ik(y \cos \alpha - x \sin \alpha)^2 / 2f] \exp(i\gamma y) \\ + \varphi(x \cos \alpha - y \sin \alpha) \exp[ik(y \cos \alpha + x \sin \alpha)^2 / 2f] \exp(-i\gamma y)$$

using a cylindrical lens, rotated by an angle α , a mirror and a prism. The setup is based on a setup in ref. 2. In eq. 1, f is the focal length of the cylindrical lens and k is the wave number of light. The two terms in eq. 1 give rise to interference effects. Using the new coordinates $x' = x \cos \alpha$, $y'/2 = y \sin \alpha$ and $\gamma' = \gamma / \sin \alpha$, the squared modulus of the field distribution, shown in fig. 2a contains the terms

$$\varphi(x'+y'/2)\varphi^*(x'-y'/2)\exp(ikx'y'/f)\exp(i\gamma'y')$$

and

$$\varphi(x'-y'/2)\varphi^*(x'+y'/2)\exp(-ikx'y'/f)\exp(-i\gamma'y')$$

By Fourier transforming the squared modulus of $\Psi(x', y')$ along the y' direction (fig. 2b), the resulting distribution contains $W'(x', p - \gamma')$ and $W'(x', -p - \gamma')$, where

$$W'(x, p) = \int \varphi(x+y/2)\varphi^*(x-y/2)\exp(ikxy/f)\exp(ipy)dy$$

is a Wigner-like, real phase-space distribution. These two terms can be spatially separated by appropriately choosing the angle γ . From the measurement of $W'(x', p)$ one can determine $\varphi(x')$, up to a constant $\varphi^*(0)$, by

$$\varphi(x')\varphi^*(0)\exp(ikx'^2/2f) = \frac{1}{2\pi} \int_{-\infty}^{\infty} W'(x'/2, p)\exp(-ipx')dp$$

The amplitude of the wave front is then directly determined from the real and imaginary parts of $\varphi(x')$, whereas the phase factor introduced by the cylindrical lens must be first subtracted in order to recover correctly the phase. In contrast to the tomographic method, only one measurement is needed in this case.

The recovered normalised amplitude profile shown in fig. 3 with a solid line, has an approximately Gaussian shape $\exp(-x^2/x_0^2)$, with $x_0 = 1.75$ mm, being in good agreement with the experimental measurement.

References

- [1] D. Dragoman, *Optics Lett.*, vol. 25, pp.281-283, 2000.
- [2] K.-H. Brenner and A.W. Lohmann, *Opt. Communications*, vol. 42, pp.310-314, 1982.
- [3] D. Dragoman, M. Dragoman, K.-H. Brenner, submitted to *Appl. Opt.* (2002)

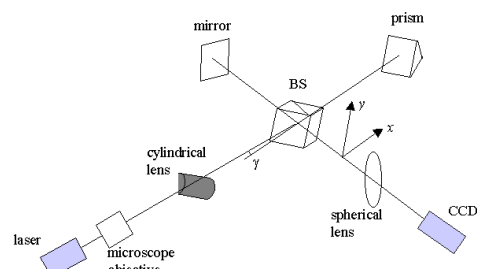


Fig. 1: Optical setup for WDF-measurement

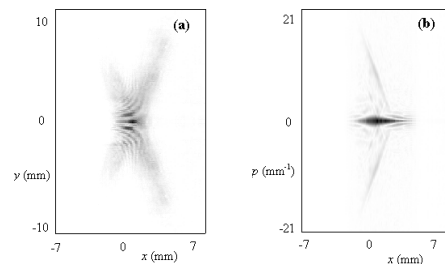


Fig. 2: (a) Measured intensity pattern, (b) computed Fourier transform.

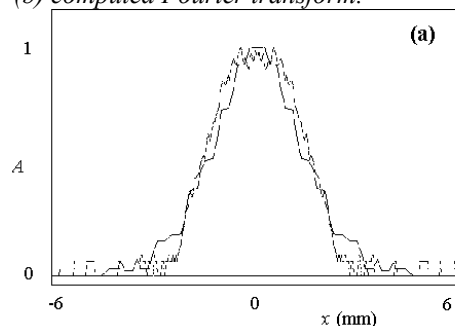


Fig. 3: Recovered normalized amplitude (solid line) and experimental normalized amplitude (dotted line).

Tomographic amplitude and phase recovery of vertical-cavity surface-emitting lasers using the Ambiguity function

D. Dragoman, M. Dragoman, K.-H. Brenner

We have investigated a non-interferometric method of determining the amplitude and phase of the wave-front of a VCSEL. The approach used here, is a tomographic method, based on the measurement of intensity in several planes along the propagation direction [1]. From these intensity measurements, the Ambiguity function (AF) [2,3] is first computed, then the amplitude and phase are retrieved from the AF via a Fourier transformation.

For a general two-dimensional wave field, the corresponding AF is four-dimensional. Therefore, in these experiments, we have chosen a wave distribution, which is separable with respect to the x and y coordinates. The measured intensity distribution in fig.1 can be approximated by a product of two 1D-distributions along the x - and y -axes, and the reference plane was not chosen at the waist of the VCSEL. Combining the definition of the AF for 1D-VCSEL beams,

$$AF(x', q; z) = \int \varphi(x + x'/2; z) \varphi^*(x - x'/2; z) \exp(-ixq) dx \quad (1)$$

with the propagation matrix and the properties of the AF:

$$\begin{pmatrix} x \\ q \end{pmatrix}_z = \begin{pmatrix} A & B \\ C & D \end{pmatrix} \begin{pmatrix} x \\ q \end{pmatrix}_0 \quad (2)$$

$$AF(Dx' - Bq, -Cx' + Aq; z) = AF(x', q; 0), \quad (3)$$

$$AF(0, q; z) = AF(-Bq, Aq; 0), \quad (4)$$

$$AF(0, q; z) = \int |\varphi(x; z)|^2 \exp(-ixq) dx, \quad (5)$$

we obtain:

$$\int I(x, z) \exp(-ixq/A) dx = AF(x' = -Bq/A, q; 0). \quad (6)$$

This means that samples of the intensity distribution taken at a series of planes z provide values of the AF along lines in phase-space. These lines, according to the matrix relation in eq.(2) make an angle θ with the q axis and satisfy $\tan \theta = -B/A$. Now from the samples of the intensity along the x axis we have computed the AF and displayed the real part in fig.2. The intensity samples that correspond to an angle $|\theta| \leq \pi/4$ were measured in free space, whereas for the angles $\pi/2 > |\theta| > \pi/4$ a combination of spherical lenses and free space was used to prevent low-intensity samples resulting from light divergence. After constructing the AF, the complex field distribution can be recovered by performing a Fourier transformation along the q axis:

$$\varphi(x) \varphi^*(0) = \int AF(x, q) \exp(ixq/2) dq \quad (5)$$

The recovered amplitude in fig. 3a is in good agreement with the experimental data, except for the outer maxima. The recovered phase, represented in Fig.3b, is almost parabolic, because the reference plane is not in the waist of the VCSEL.

References

- [1] D. Dragoman, M. Dragoman, K.-H. Brenner, submitted to Opt. Letters (2002)
- [2] K.-H. Brenner, A.W. Lohmann, J. Ojeda-Castaneda. Opt. Comm. **44**, 323 (1983)
- [3] D. Dragoman, M. Dragoman, K.-H. Brenner. Appl. Opt. **39**, 2912 (2000)

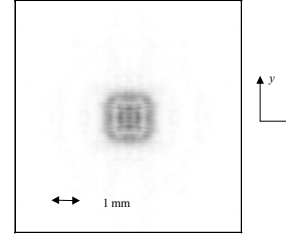


Fig. 1: Intensity distribution in a plane z

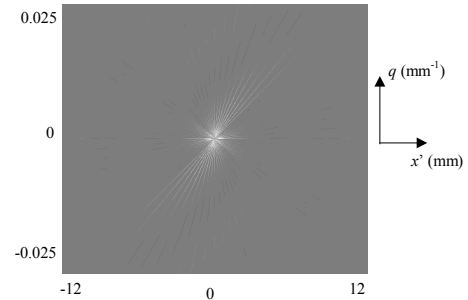


Fig. 2: $Re(AF)$ of intensity samples

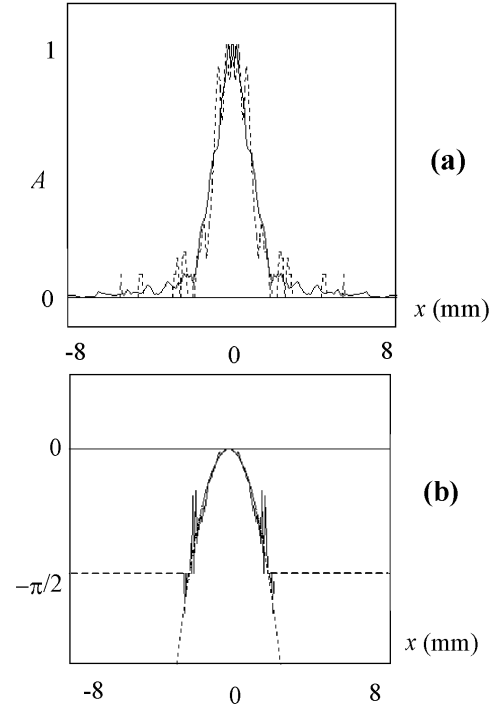


Fig. 3: (a) Recovered (solid line) versus experimental (dotted line) amplitude profile. (b) Recovered phase profile (solid line) and the best fit parabola (dotted line)

List of recent publications

77. U.-W. Krackhardt, R. Klug, K.-H. Brenner, "Broadband parallel fiber optical link for short distance interconnection with multi-mode fibers", *Appl. Opt.* **39**, No. 5, 690 - 697, (2000)
78. K.-H. Brenner, R. Klug, A. Knüttel, "Microoptic Implementation of an Array of 1024 Confocal Sensors", in *OPTO '98 Proceedings*, AMA Fachverband für Sensorik, 155 -160, Erfurt (1998)
79. K.-H. Brenner, U.W. Krackhardt, R. Klug, "Directional Multiplexing for optical Board to Board Interconnections", in *Optics in Computing '98*, Proceedings of SPIE **3490**, 416 - 418, Bruegge (1998)
80. J. Bähr, K.-H. Brenner, "Optical motherboard: a planar chip to chip interconnection scheme for dense optical wiring", in *Optics in Computing '98*, Proceedings of SPIE **3490**, 419 - 422, Bruegge (1998)
81. K.-H. Brenner, "Analysis of phase anomalies and design of continuous phase elements", in *Diffraction Optics '99*, EOS Topical Meeting Digest Series **22**, ISSN 1167-5357, 22 - 23, Jena (1999)
82. U. W. Krackhardt, K.-H. Brenner, "Forward Construction of HOEs by Continuous Aperture Division", in *Diffraction Optics '99*, EOS Topical Meeting Digest Series **22**, ISSN 1167-5357, 163 - 164, Jena (1999)
83. K.-H. Brenner, "Method for designing arbitrary two-dimensional continuous phase elements", *Opt. Lett.* **25**, No. 1, 31 - 33, (2000)
84. U. W. Krackhardt, R. Klug, K.-H. Brenner, "Faser-optische Kurzstreckenverbindungen zur breitbandigen und parallelen Signalübertragung", *ORT 1999*, Tagungsband 4. Workshop Optik in der Rechentechnik, ISSN 1437-8507, 10 - 15, Jena (1999)
85. J. Bähr, K.-H. Brenner, J. Moisel, W. Singer, S. Sinzinger, T. Spick and M. Testorf, "Modification of the imaging properties of ion-exchange microlenses by mask shaping", in Technical Digest of the Tenth Topical Meeting on Gradient-Index Optical Systems, (European Optical Society, 1992), p. 187, Santiago de Compostela, Spain, 4-6- Oct. 1992
86. Krackhardt, Ulrich, Dr., 68199 Mannheim; Brenner, Karl-Heinz, Prof. Dr., 68309 Mannheim, "Absolutes flächenhaftes Interferometer", Anmeldetag 24.07.1998, DE 198 33 291 A1, IPC G 01 B 9/02
87. U. W. Krackhardt, R. Klug, K.-H. Brenner, "Demonstration of a parallel optical transmission using angle multiplexing in optical fibres", *Optics in Computing 2000*, Roger A. Lessard, Tigran Galstian, Editors, Proceedings of SPIE, Vol. **4089**, 86 - 92, ISBN 0-8194-3732-8, ISSN 0277-786X, Quebec City, Canada (2000)
88. K.-H. Brenner, J. Bähr, T. Schmelcher, "Design and Fabrication of arbitrary , non-separable continuous phase elements", in *Diffraction Optics and Micro-Optics*, OSA Technical Digest, 237 - 239, ISBN 1-55752-635-4, Quebec City, Canada (2000)
89. U. W. Krackhardt, R. Klug, and K.-H. Brenner, "Multimode Fiber Interconnect for Parallel, High Bandwidth - Short Distance Data Link, in *Progress in Electromagnetics Research Symposium (PIERS)*, The Electromagnetics Academy, PIERS 2000 Proceedings, 726, ISBN 0-9679674-0-6, Cambridge, Massachusetts, USA (2000)
90. Daniela Dragoman, Mircea Dragoman, and Karl-Heinz Brenner, "Optical realization of the ambiguity function of real two-dimensional light sources", *Applied Optics* **39**, No. 17, 2912 - 2917, (2000)
91. INVITED: Karl-Heinz Brenner, "Development of modules for micro optical integration and MOEMS packaging", in *MOEMS and Miniaturized Systems*, Eds: M. Edward Motamedi, Rolf Göring, Proceedings of SPIE, Vol. **4178**, 138 - 140, ISSN 0277-786X, Santa Clara, USA (2000)
92. P. Kümmel, U. Krackhardt, K.-H. Brenner, S. Dambach, "Berechnung und Herstellung mikrooptischer Elemente für den blauen DVD-Standard", 5. Workshop Optik in der Rechentechnik, Tagungsband, eds.: Stefan Sinzinger, Jürgen Jahns, 69 - 73, ISSN 1437-8507, Hagen (2000)

93. U. W. Krackhardt, R. Klug, K.-H. Brenner, "Realisation and Application of a parallel high-bandwidth Interconnect over a single multimode Fibre by Angle Division Multiplexing", in *14th International Conference on Optical Fiber Sensors*, A.G. Mignani, H.C. Lefèvre, Editors, Proceedings of SPIE, Vol. **4185**, 174 - 177, ISSN 0277-786X, Venedig (2000)
94. J. Bähr, T. Schmelcher, K.-H. Brenner, "Tolerant Coupling of integrated Multimode Waveguides", in *LEOS 2000*, IEEE Annual Meeting Conference Proceedings, Vol. **2**, 571 - 572, ISBN 0-7803-5947-X, Puerto Rico (2000)
95. J. Bähr, K.-H. Brenner, "H-ROD: A new and versatile microoptical component", *OPTIK* **112**, No 7, 289 – 294, (2001)
96. Jochen Bähr, Thilo Schmelcher, Karl-Heinz Brenner, "Tolerant Coupling of integrated Multimode Waveguides", in *Optics in Computing*, OSA Technical Digest, 116 – 118, ISBN 1-55752-656-7, Lake Tahoe/Nevada (2001)
97. U. Krackhardt, R. Klug, K.-H. Brenner, "Angle Division Multiplexing: Investigation of the multiplexing potential of real systems", *ORT 2001*, Proceedings 6th Workshop Optics in Computing Technology, 101 – 108, ISSN 1437-8507, Paderborn (2001)
98. T. Schmelcher, J. Bähr, K.-H. Brenner "Tolerant Coupling of integrated Multimode Waveguides", *ORT 2001*, Proceedings 6th Workshop Optics in Computing Technology, ISSN 1437-8507, 87 – 91, Paderborn (2001)
99. Ulrich Krackhardt, Karl-Heinz Brenner, „Integrated Guiding Structures for automatic Alignment of micro optical Components“, *SPIE 46. Annual Meeting, Gradient Index, Miniature, and Diffractive Optical Systems II*, Proceedings of SPIE, Vol. **4437**, 91 – 98, ISSN 0277-786X/01, San Diego (2001)
100. Jochen Bähr, Karl-Heinz Brenner, „Realization of refractive continuous phase elements with high design freedom by mask structured ion exchange“, *SPIE 46. Annual Meeting, Gradient Index, Miniature, and Diffractive Optical Systems II*, Proceedings of SPIE, Vol. **4437**, 50 – 60, ISSN 0277-786X/01, San Diego (2001)
101. Karl-Heinz Brenner, Peter Kümmel, Uwe Zeitner, „Design, analysis and fabrication of refractive beam shaping elements for optical storage applications“, *SPIE 46. Annual Meeting, Laser Beam Shaping II*, Proceedings of SPIE, Vol. **4443**, 93 – 104, ISBN 0-8194-4157-0, San Diego, USA (2001)
102. INVITED: Karl-Heinz Brenner, „Image formation by beam shaping. Design methods and applications“, Workshop Optics for Information Systems, *4th Euro-American Workshop, Optoelectronic Information Processing: Optics for Information Systems*, Critical Reviews of Optical Science and Technology, Vol. **CR81**, 1 – 12, ISBN 0-8194-4123-6, Valencia, Spain (2001)
103. INVITED: J. Bähr, U. Krackhardt, K.-H. Brenner „Fabrication and Testing of planar Micro Lens Arrays by Ion Exchange Technique in Glass“, *SPIE 46. Annual Meeting, Workshop on Microlens Measurement Standardization*, San Diego, USA, to appear in SPIE Proceedings (2001)
104. W. Singer, K.-H. Brenner "Stacked Micro-optical Systems" in *Micro-optics, Elements, systems and applications*, ed. H.P. Herzig, Taylor & Francis Ltd. London, 199 - 221, ISBN 0-7484-0481-3 (1997)
105. D. Dragoman, M. Dragoman, K.-H. Brenner " Tomographic amplitude and phase recovery of vertical-cavity surface emitting lasers using the ambiguity function", *OSA/Optik Letters*, submitted (2002)